Traditional Journal of Multidisciplinary Sciences (TJMS)

January-June 2023, Vol. 01, No. 01, [73 – 92]

Published: 30th June 2023

https://ojs.traditionaljournaloflaw.com/index.php/TJMS

RESEARCH PAPER

Synthesis and Deposition of ZnO NRs/TiO_2 on Zinc Oxide Seed Layer for Dye Synthesize Solar Cell

Salisu I. Kunya[1] Yunusa Abdu[2] Mohd Kamarulzaki Mustafa[3] Mohd Khairul Ahmad[4] A. O. Musa[5]

[1] Universiti Tun Hussein Onn Malaysia (UTHM), Malaysia
[1,2] Bayero University, Kano, Nigeria
[3-4] Universiti Tun Hussein Onn Malaysia (UTHM), Malaysia
[5] Bayero University, Kano, Nigeria

**Corresponding Author* *salisukunya2016@gmail.com*

ABSTRACT

Dye synthesis solar cells (DSSCs) are an innovative method of generating electricity, but their efficiency lags behind that of silicon solar cells. Numerous strategies have been explored to enhance DSSC performance to address this issue, such as employing nanorods to boost the electron transport rate in photoanodes, doping materials with different ions, and developing tandem DSSCs. This study focuses on synthesizing and depositing a ZnO nanorods (NRs) and TiO2 (ZT) photoanode on a zinc oxide seed layer. ZnO nanoparticles and nanorods were created using spin coating and hydrothermal methods. The growth of vertically aligned nanorods serves to enhance the electron transport rate, with the seed layer precursor concentration influencing the nanorod morphology. The morphology, structure, optical properties, and electrical properties were evaluated using field emission scanning electron microscopy (FESEM), X-ray diffraction (XRD), UV-visible spectrometer, and solar simulator. Electron microscope images exhibit nanorods, nanoparticles, and other structures generated through hydrothermal methods. XRD analysis confirms the presence of crystalline zinc oxide and TiO2 in the synthesized materials. The optical band-gap of ZT-1.0M is determined to be 3.84 eV, while that of ZT-0.7M is 3.924 eV, suggesting a larger band-gap value for the latter, possibly due to variation in crystalline size. The conversion efficiency of DSSC is observed to be 0.7645% for ZT-1.0M and 0.6469% for ZT-0.7M, indicating an improvement in performance.

Keywords: DSSC, hydrothermal, TiO2, ZnO NRs

INTRODUCTION

According to Tyagi et al. (2021), the generation of sustainable energy is a crucial step in meeting current energy demands without jeopardizing the ability of future generations to meet their own needs. In Africa, energy poverty significantly hinders the region's development potential, as highlighted by Adams and Nsiah (2019). The combination of population growth and heavy

reliance on fossil fuels as the primary energy source in the region has led to increased carbon dioxide emissions, resulting in detrimental environmental impacts. Rahman et al. (2017) emphasize the multiple benefits of renewable energy, particularly its capacity to reduce carbon dioxide emissions. Consequently, global attention is shifting toward clean energy solutions in order to decrease humanity's dependence on fossil fuels, as highlighted by Mehmood et al. (2017). The utilization of photovoltaic technology for directly capturing solar energy is gaining significant attention as a crucial element in the future global energy landscape. Over the years, there have been substantial advancements and transformations in solar PV technologies, as highlighted by Sugathan et al. (2015). One promising avenue within this field is dye-sensitized solar cells (DSSCs), which offer a distinctive opportunity to fine-tune both the light absorption and charge-transport processes occurring within the cell. In their literature, Sharma et al. (2017) discuss the potential for enhancing the efficiency of DSSCs by enhancing photon absorption in a specialized manner. This situation presents exciting possibilities to concentrate research efforts on the active material component of DSSCs, specifically the photoanode. The photoanode is a crucial element as it accommodates the dye and facilitates the transfer of electrons. Achieving a rapid electron transport rate within the electrode can greatly enhance the cell's performance, as Yan et al. (2012) emphasized.

Investigating semiconductor materials at the nanostructure level is important due to their unique physicochemical characteristics, which differ from their bulk counterparts, as highlighted by Ali et al. (2015). Zinc oxide (ZnO) is a polar crystal that typically exhibits n-type semiconducting properties, with its conductivity type being linked to inherent defects within the material, as Inamdar et al. (2014) explained. When observed at the nanoscale, ZnO manifests as wire-like structures and rods, as Edalati et al. (2016) described. Similarly, titanium oxide (TiO_2) possesses negative conductivity due to its intrinsic defects, as Dodoo-Arhin et al. (2018) discussed. TiO_2 exists in three crystalline states, each with slightly different band-gap energies, as Humayun et al. (2018) indicated. The literature suggests that TiO_2 phases exhibit efficient responses to ultraviolet irradiation, as Tiwari et al. (2019) demonstrated. Parisi et al. (2017) have extensively acknowledged the exceptional semiconductor properties of both titanium oxide (TiO_2) and zinc oxide (ZnO), particularly in their application as photoanodes and electron transporters. These materials possess desirable electronic, electrical, and luminescent properties, along with strong absorption capabilities in the ultraviolet (UV) region and high transparency in the visible region, as Zainal et al. (2018) highlighted.

Despite these favorable attributes, ZnO-based dye-sensitized solar cells (DSSCs) still pose challenges and require further investigation to enhance their photovoltaic properties. Consequently, there is a need to explore the synthesis of materials such as rods, wires, and nanotubes (NTs) in order to achieve enhanced electron transport within the photoelectrode. This is attributed to the uninterrupted movement of photo-generated electrons facilitated by these nanostructures, as discussed by Al-Kahlout (2015). A study conducted by John K. et al. (2016) involved the creation of a heterostructure using ZnO nanorods and TiO_2 to enhance performance. This was possible due to the favorable compatibility between TiO_2 and ZnO and their similar band alignments. Incorporating ZnO nanorods improved the flow of charge carriers and reduced recombination, while TiO_2 particles were utilized to enhance dye absorption. The researchers

opted for the hydrothermal method as it offered several advantages, including the availability of necessary equipment (Ejovwokoghene et al., 2020). Hydrothermal synthesis of ZnO nanorods involves a bottom-up approach where zinc salts and other chemicals capable of producing hydroxyl ions are employed to facilitate the reaction's completion.

Operation of dye-synthesized solar cells

Dye-sensitized solar cells (DSSCs) undergo three crucial processes: absorption, separation, and collection of charges, as described by Iqbal et al. in 2019. These processes are fundamental to the functioning of DSSCs. The absorption process refers to the initial step in which a dye layer within the cell captures photons from sunlight. Once absorbed, the separated charges need to be efficiently separated within the cell. This separation process allows the positive charges (holes) and negative charges (electrons) to move in opposite directions, thus preventing recombination and maximizing the cell's efficiency. The collection process involves capturing and channeling the separated charges to their respective electrodes.

The energy of the photons interacting with the DSSC is a concept initially explained by Max Planck and later elucidated by Albert Einstein, as referenced by Akinoglu et al. in 2021.

$$Ep=hc/\lambda \quad (1)$$

where h represents the Planck constant ($h = 6.626x10^{-34}$ J·s), ν represents the frequency of the photon, λ represents its wavelength, and c represents the speed of light.

When photons from a light source come into contact with the colorant, the colorant initially absorbs the photons. This absorption process causes the particles within the colorant to transition from one energy state to another, becoming energized.

$$h\nu+D\rightarrow D^* \quad (2)$$

After being energized by the absorbed photons, the particles in the dye undergo a subsequent step in which they are driven or pushed into the ZnO nanorods (ZnO NRs) and TiO_2 layers, subsequently to the flow through an external circuit toward the opposite electrode.

$$D^*\rightarrow D^+ + e^- \ (semiconductor) \quad (3)$$

During the operation of a dye-sensitized solar cell (DSSC), when an electron is lost from the dye molecule after absorbing a photon, it is replenished through the process of taking particles from the redox mediator. The redox mediator, typically a solution or electrolyte present within the DSSC, donates an electron to the dye molecule. The redox mediator acts as an electron donor, replenishing the lost electron and maintaining the balance of charges within the system. This process takes place through the collection of electrons from the opposite electrode. By collecting electrons from the opposite electrode, the redox mediator maintains a cycle of electron transfer in the DSSC.

$$2D^*+3I^- \rightarrow 2D+I_3^- \quad (4)$$

This process ensures a continuous supply of electrons to the dye molecule, allowing for sustained photon absorption and electron flow.

$$I_3^- + 2e^- \text{ (Counter electron)} \rightarrow 3I^- \quad (5)$$

At last, the steps were happening again several time.

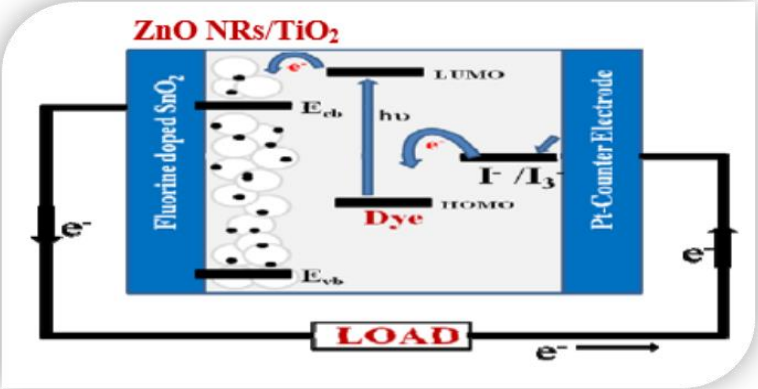

Figure 01. Schematic diagram of ZnO NRs/TiO_2 DSSC

MATERIAL AND METHODS

Materials

The materials necessary in this work are diethanolamine $HN(CH_2CH_2OH)$, Zinc acetate dihydrate $(Zn(CH_3COO)_2.(H_2O)_2)$, Hexamethylenetetramine $(C_6H_{12}N_4)$, Water (H_2O), Iodine tri-iodide, ethanol (CH_2CH_2OH), Titanium tetraisopropoxide $(C_{12}H_{28}O_4Ti)$, zinc nitrate hexahydrate $(Zn(NO_3)_2 \cdot 6H_2O)$, N719 dye, FTO glass substrate, spin coater, stopwatch, autoclave, adhesive tape, beaker.

Preparation and deposition of ZnO film seed layer

The work is of four steps as follows.

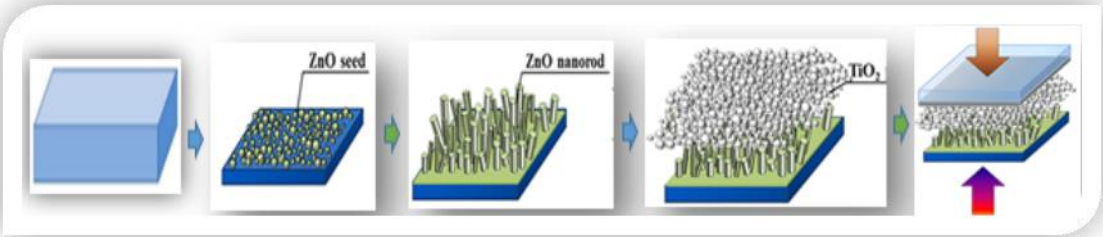

Figure 02. Schematic for the deposition of ZnO seed layer (SL), ZnO nanorods on SL, TiO_2 on the ZnO and DSSC (Song et al., 2014)

The FTO-coated glass substrates were ultrasonically cleaned in deionized water, acetone, ethanol, and deionized water, each for 10 minutes, and then dried. Spin-coating processes were used specifically for the deposition of the ZnO layers. Prior to the deposition of ZnO film, a 0.4 M solution concentration of ZnO was prepared by dissolving zinc acetate dihydrate ($Zn(CH_3COO)_2 \bullet 2H_2O$) and stabilizing agent, i.e., diethanolamine $HN(CH_2CH_2OH)$ in 10mL ethanol (CH_2CH_2OH). The solution was agitated on a hot plate stirrer for 30 minutes at 60 °C and subsequently for 24 hours at room temperature to achieve a homogenous solution. The resultant solution was dropped on a clean substrate and spun for 30 minutes at a speed of 3000 rpm. The coated glass substrate was then dried at 100 °C for 1 minute to allow the solvent to evaporate. To obtain the necessary thickness, the coating process was repeated five times. The seed layer is then heated for 1 hour at 450 °C. This step is required to prevent the seed layer from dissolving into the growth solution and improve the grown nanorods' vertical alignment (Hezam et al., 2021). In an effort to obtain dense and uniform ZnO nanorods arrays. Another ZnO seed solution were prepared at 0.7, 1.0, and 1.3 M, and the ratio of zinc acetate dihydrate and diethanolamine in the chemicals bath was maintained as (1:1). The deposition process was repeated for these solutions.

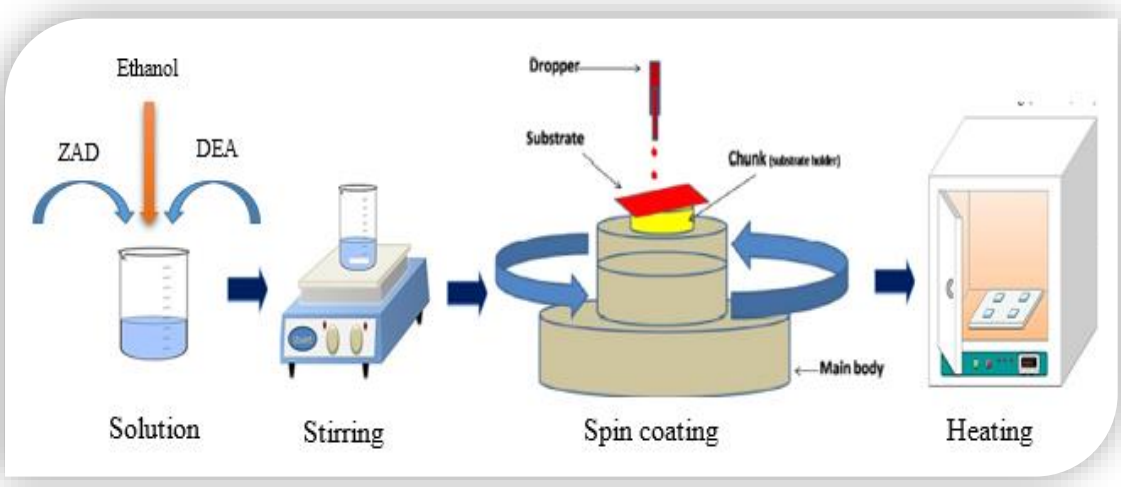

Figure 03. Schematic diagram of the Seeding process.

Preparation and deposition of ZnO nanorods

The growth of ZnO nanorods was achieved using a hydrothermal method, which involved several steps. To prepare the growth nutrient solution, 1.48g of zinc nitrate hexahydrate ($Zn(NO_3)_2 \cdot 6H_2O$) and 0.7g of hexamethylenetetramine ($C_6H_{12}N_4$) were dissolved in 100mL of deionized water in a beaker, resulting in a 0.05 M concentration.

After stirring the solution for 15 minutes to ensure a uniform mixture, it was transferred to an autoclave. Inside the autoclave, a ZnO seed layer, previously prepared from zinc acetate at a concentration of 0.4 M, was placed approximately 450 from the wall. The autoclave was then placed in an oven and maintained at a temperature of 150°C for a duration of 3 hours. Following hydrothermal, the resulting ZnO nanorods were carefully removed from the autoclave. They were subsequently cleaned with deionized water to remove impurities and moisture, ensuring their

purity and stability in ambient air conditions. The entire procedure was repeated using ZnO seed layers prepared from zinc acetate dihydrate at concentrations of 0.7 M, 1.0 M, and 1.3 M to explore the effects of different seed layer concentrations.

In summary, a hydrothermal method was utilized to grow ZnO nanorods. This involved preparing a growth nutrient solution, transferring it to an autoclave containing a ZnO seed layer, subjecting it to a controlled temperature and time in an oven, and cleaning and drying the resulting nanorods. The process was repeated with varying concentrations of the ZnO seed layer to study their impact on growth.

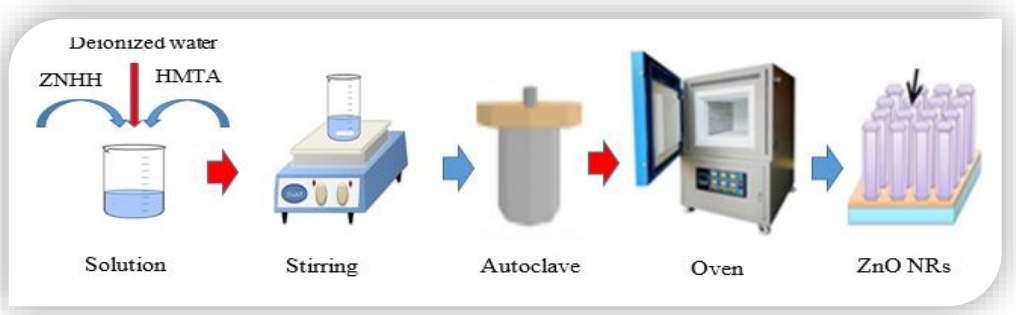

Figure 04. Schematic diagram of ZnO nanorods growth.

Growing ZnO nanorods (ZnO NRs) involves a specific mechanism. Initially, in an aqueous solution, zinc nitrate hexahydrate ($Zn(NO_3)_2 \cdot 6H_2O$) and hexamethylenetetramine (HMTA) undergo decomposition, resulting in the release of specific ions.

The decomposition of zinc nitrate hexahydrate and HMTA in the aqueous solution releases Zn^{2+} and OH^- ions, respectively. These ions serve as crucial components for the subsequent growth of ZnO nanorods, providing the necessary building blocks and participating in the reaction processes involved.

$$Zn(NO_3)_2.6H_2O \rightarrow Zn^{2+} + 2NO_3^- + 6H_2O \quad (6)$$

$$NO_3^- + H_2O + 2e^- \rightarrow NO_2^- + 2OH^- \quad (7)$$

In our particular scenario, hexamethylenetetramine (HMTA) serves as a source of OH^- ions, which plays a crucial role in accelerating the nucleation and growth of ZnO nanorods. The initial step involves the thermal degradation of HMTA, resulting in the formation of formaldehyde and ammonia. Subsequently, hydroxyl ions are released through the hydrolysis process of HMTA. During the thermal degradation of HMTA, the compound undergoes a chemical transformation due to the applied heat. This process leads to the breakdown of HMTA molecules, resulting in the generation of formaldehyde and ammonia. These byproducts play a part in subsequent reactions that facilitate the release of hydroxyl ions. Hydroxyl ions are formed through the hydrolysis of HMTA. This hydrolysis process involves the interaction between water molecules and the degraded HMTA molecules. As a result, hydroxyl ions (OH^-) are released into the solution,

contributing to the overall concentration of OH^- ions available for the growth of ZnO nanorods. By providing a source of OH^- ions, HMTA enhances the nucleation and growth of ZnO nanorods. The presence of OH^- ions promotes the formation of ZnO nuclei and facilitates their subsequent growth into nanorods during the hydrothermal synthesis process.

$$(CH_2)_6N_4 + 6H_2O \rightleftharpoons 6COH_2 + 4NH_3 \quad (8)$$

$$NH_3 + H_2O \rightleftharpoons NH4^+ + OH^- \quad (9)$$

When the concentration of Zn^{2+} and OH^- reach the supersaturation critical value, they combine to form fine ZnO particles in the aqueous solution.

$$2OH^- + Zn^{2+} \rightarrow Zn(OH)_2 \quad (10)$$

$$Zn(OH)_2 \rightarrow ZnO + H_2O \quad (11)$$

The morphological growth of ZnO nanorods can be explained through the processes of nucleation, rearrangement, and growth, as described by Rui et al. in 2017. During the nucleation stage, a significant number of ZnO nuclei are formed, exhibiting homogeneity in their distribution. Following nucleation, the nanoparticles undergo a rearrangement phase, regrouping and aligning to form nanochains. These nanochains serve as the building blocks for the subsequent growth of the nanorods. Finally, in the growth period, the nanorods experience preferred anisotropic growth along the desired direction of ZnO, resulting in their characteristic elongated shape.

To visually represent this growth process, Figure 8 presents a photographic depiction or illustration showcasing the stages of nucleation, rearrangement, and growth. The figure serves as a model or visual reference for understanding the morphological development of ZnO nanorods. In summary, the growth of ZnO nanorods involves the formation of ZnO nuclei during nucleation, followed by a rearrangement phase where nanoparticles align to form nano chains. Finally, the nanorods undergo a preferred anisotropic growth, resulting in their distinctive elongated structure. Figure 8 provides a visual representation of this growth process.

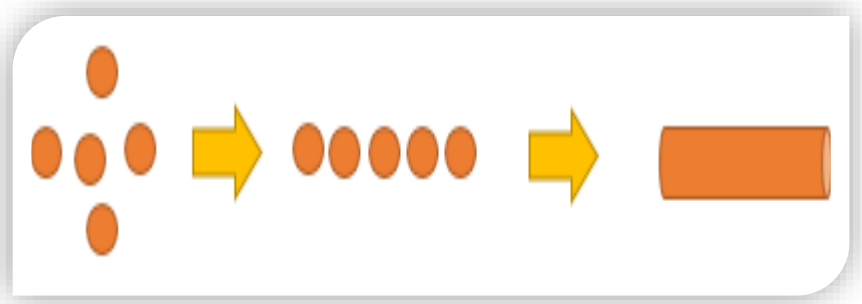

Figure 5. The photograph descriptions of ZnO nanorods' evolution

Preparation and deposition of TiO_2

A method was employed to synthesize nanostructured TiO_2, which involved a series of steps. To begin, 3 ml of titanium isopropoxide and 5.5 ml of acetic acid were combined in a clean beaker. To this mixture, 10 ml of 2-propanol and 3 ml of water were added. Additionally, a small amount of triton X-100, serving as a surfactant, was included. The entire mixture was stirred continuously for one day, resulting in the formation of a gel-like substance. Next, the deposition process was initiated by spraying an appropriate quantity of the solution onto the ZnO nanorods (ZnO NRs), which were placed on a hot plate set to a temperature of 1000 °C. This quick drying step facilitated the adhesion of the TiO_2 onto the ZnO NRs. Subsequently, the entire photoanode structures were subjected to further drying. They were placed inside a furnace and maintained at a temperature of 450 °C for a duration of one hour. This step ensured the complete drying and stabilization of the photoanodes. A visual representation of the processes involved in the fabrication of the photoanodes can be observed in Figure 2, providing a model that illustrates the sequence of steps for creating the photoanodes. The synthesis of nanostructured TiO_2 involved mixing titanium isopropoxide and acetic acid, followed by the addition of 2-propanol, water, and a surfactant. After the formation of a gel-like substance through continuous stirring, the solution was sprayed onto ZnO NRs and subjected to drying on a hot plate. The final step involved drying the photoanodes in a furnace. The processes were visually depicted in Figure 2, showcasing the sequence of steps for creating the photoanodes.

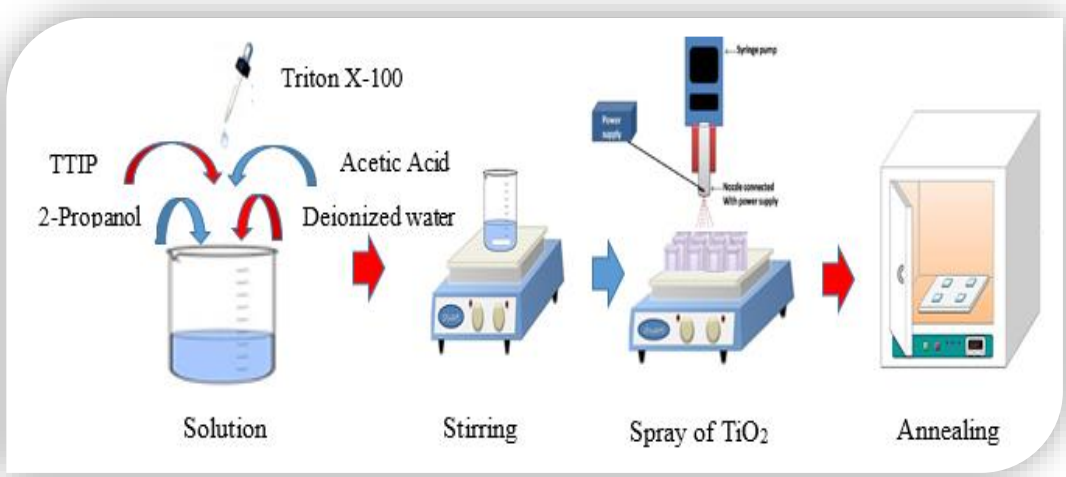

Figure 6. Schematic diagram of TiO_2 spraying

Fabrication of DSSC

The photoanode was oriented upward, with the conductive side of the Pt-coated counter electrode facing the photoanode. Capillary action was used to introduce liquid electrolytes into the gap between the photoanode and the counter electrode (cathode) to create a DSSC. The two electrodes were fastened with two binder clips to establish dye-manufactured solar cells to prevent electrolyte leakage.

RESULTS AND DISCUSSION

Morphological analysis

The prepared samples were subjected to field emission scanning electron microscopy (FESEM) measurements.Their corresponding morphologies at 100KX magnification are presented in Figure 7 (a) – (d). The grown material is a micro nanostructure with a unique morphology, as shown in Figure 7 (a). This morphology was observed to have an irregular and interconnected sheet structure similar to that of ginger root. The shape could be explained by lateral crystal growth being faster than vertical growth. As shown in Figure 7 (b), the FESEM image of the sample grown on a seed layer prepared at 0.7M revealed that the sample comprises aggregates of small, irregularly shaped particles of varying sizes. Figure 7 (c) shows a dense and well-crystallized nanorod formed in a 1.0M precursor solution; the identified good quality hexagonal ZnO nanorods are due to an improved Zn^{2+} and OH^{2-} species, all through hydrothermal processes. As a result, the ability to form a uniform and dense thin layer of nanorods is of paramount significance in the fabrication of high-performance DSSCs since it is able to reduce charge recombination while offering a direct path for the flowing electrons. The nanorods morphology is comparable to the research of (Mustafa et al., 2017), who used a similar method to synthesize ZnO. Synthesis of seed layer at 1.3M, exposed stacked and overlapped nanorods. From these results, it is possible to conclude that proper optimization of the seed layer controls the orientation of ZnO NRs.

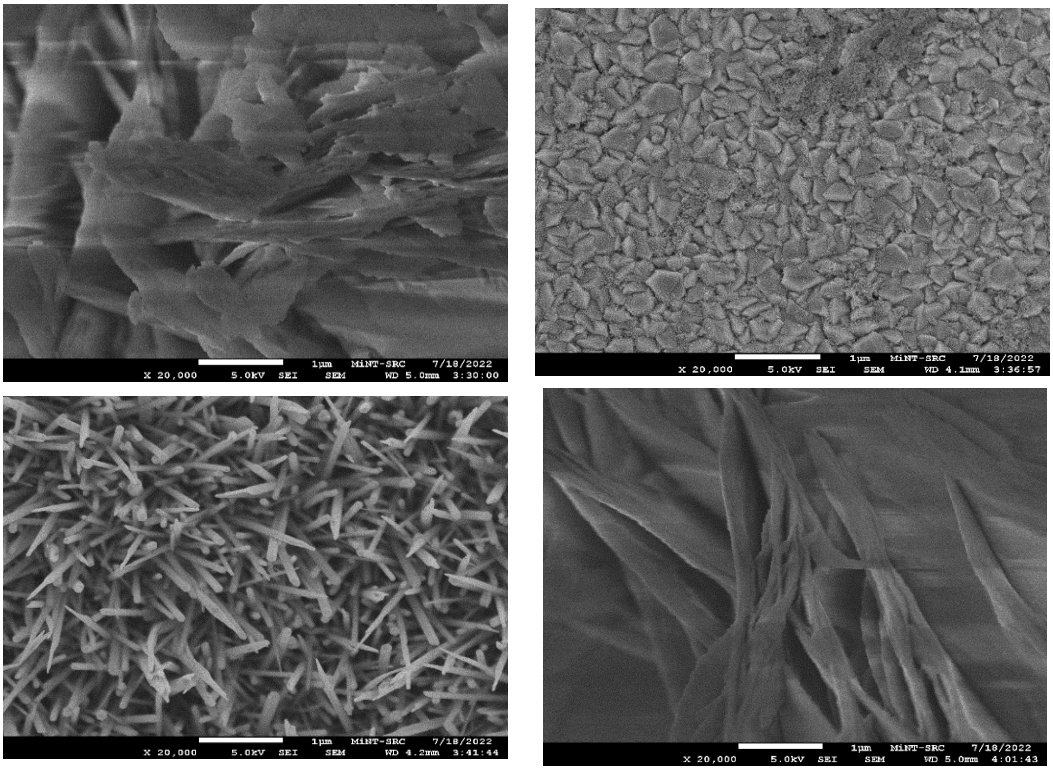

Figure 7. FESEM image of ZnO nanorods grown from seed layer of (a) 0.4M (b) 0.7M (c) 1.0M (d) 1.3M

The histograms of particle size distribution are shown in Figure 8. It provides information about the variation of nanoparticle size. The histogram clearly indicated that the average particles

size found using image j software is around 72.38 nm, while the average diameter is approximately 69.6 nm.

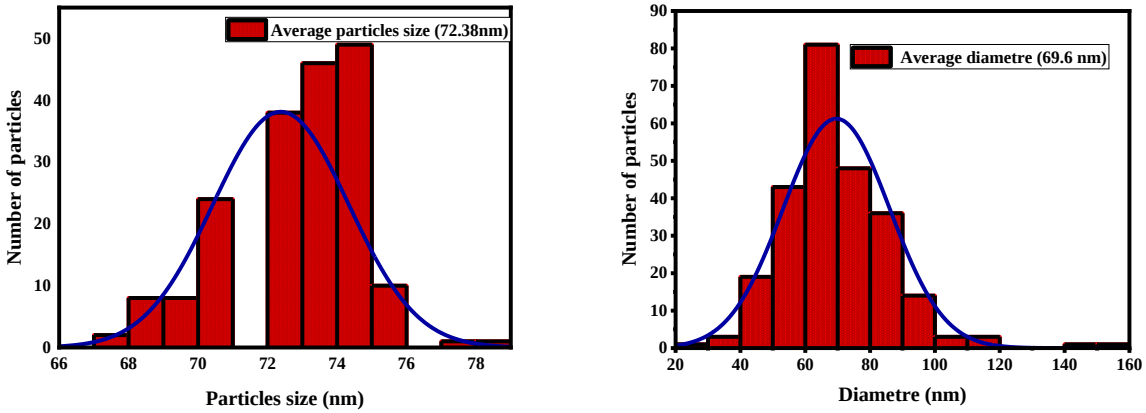

Figure 8. Histogram presenting (a) Particles size of ZnO (b) Diametre of ZnO Nanorods

It was noticed in Figures 7 (a) and (d) that there was no presence of ZnO nanorods; as a result, no further characterization was conducted on them. But film using other concentration display particles and nanorods morphology; thus, further characterization was performed for the purpose of comparison. To improve the dye absorption of the photoanode, TiO_2 was sprayed on ZnO films. As seen in Figure 9 (a), the outer TiO_2 completely covers the underlayer, and the image possesses highly densely packed nanoparticles with many spaces; this allows sufficient dye absorption (Tan et al., 2021). In the case of deposition of TiO_2 on ZnO nanorods, the surface future was preserved, but the sizes of nanorods increased more spacious to allow sufficient light trapping, scattering, and absorption.

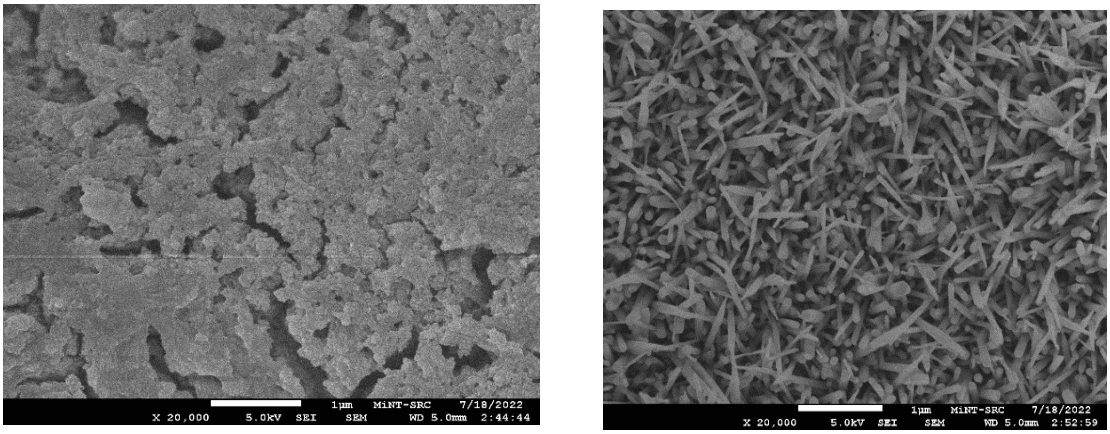

Figure 9. FESEM image of ZnO NRS – TiO_2 composite grown from seed layer of (a) 0.7M and (b) 1.0M

The cross-section view of ZnO and ZnO/TiO_2 is presented in Figure 10. The picture convinced the perpendicular nature of nanorods. The measured length of the nanorod arrays calculated using Image J software is in the range of 480 - 600nm. After spraying TiO_2 on top, the nanorods' height varies due to the falling down of some rods due to the high density of TiO_2. One can see that combining nanorods with TiO_2 nanoparticles has benefits in the sense that ID structure would improve conductivity, whereas TiO_2 resulted in high dye adsorption (Maçaira et al., 2013), (Boro et al., 2018). Chou et al. (2019) synthesized TiO_2 on top of ZnO nanorods for solar cells, and 4.73% was realized.

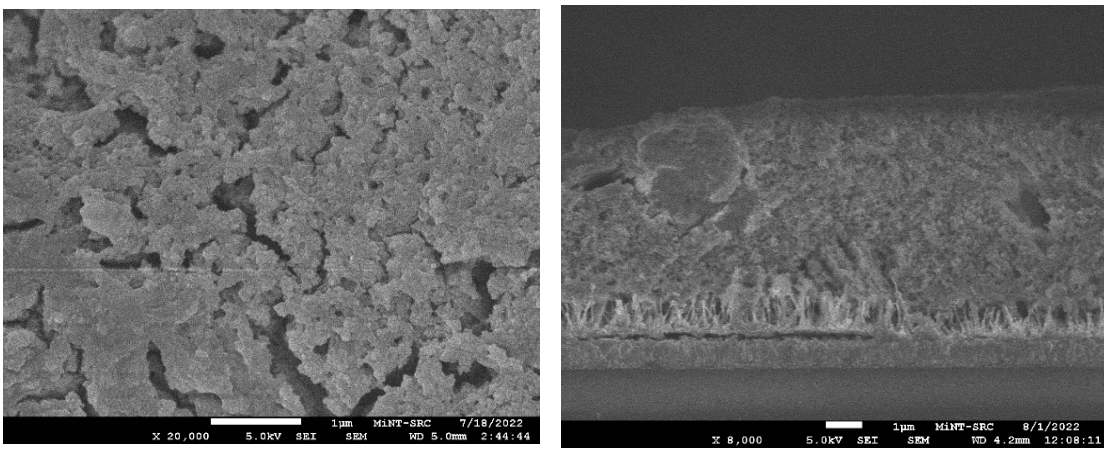

Figure 10. FESEM cross-section image of ZnO NRS – TiO_2 composite (a, b) at (1.0M)

XRD analysis

The synthesized nanocomposite was subjected to XRD analysis to confirm the product's phase. As a reference, Ossai et al., (2020) have shown that the XRD pattern for ZnO has a sharp peak of (002) at 34.28. And according to Bakr et al., (2017) the highest and strongest peak (101) of TiO_2 is at 25.4. The XRD spectra of the presence work is shown in Figure 11. All peaks come from the diffraction of different crystal planes of ZnO and TiO_2. This means that the prepared samples contain both ZnO and TiO_2. The XRD patterns of the samples show significant differences after changing the precursor concentration of the seed layer. The nature of reflection peaks from both ZnO and TiO_2 shows it is crystalline. The peaks of nanorods match with JCPDS Card file no. 36-1451 proved to be hexagonal structure while anatase phase was confirmed and matched with JCPDS card No. 00-021-1272. Thus the reflections corresponding to the other TiO_2 polymorphs are absent. The result is in agreement with the findings of Mousa et al., (2021), where all characteristic peaks of both TiO_2 and ZnO were observed. The determination of the crystallite size from the highest diffraction peak was quantified using Scherer's equation (Khalid Hossain et al., 2017)

$$D = \frac{0.9\lambda}{\beta cos\theta} \tag{12}$$

Where θ is the Bragg diffraction, λ is the wavelength of CuKα, and β is the full width at half maximum (FWHM) intensity of the XRD peak.

The estimated average crystalline size ranges are 14.42 and 13.48 nm, respectively, for ZT -1.0M and ZT – 0.7M. We know that larger crystallite sizes result in superior electron transport in photoanodes (Zatirostami, 2021). In addition, the crystallite size has an eminent control on the absorption and thus in the achievement of DSSC due to the fruitful surface area of adsorption (Rajan and Cindrella, 2019).

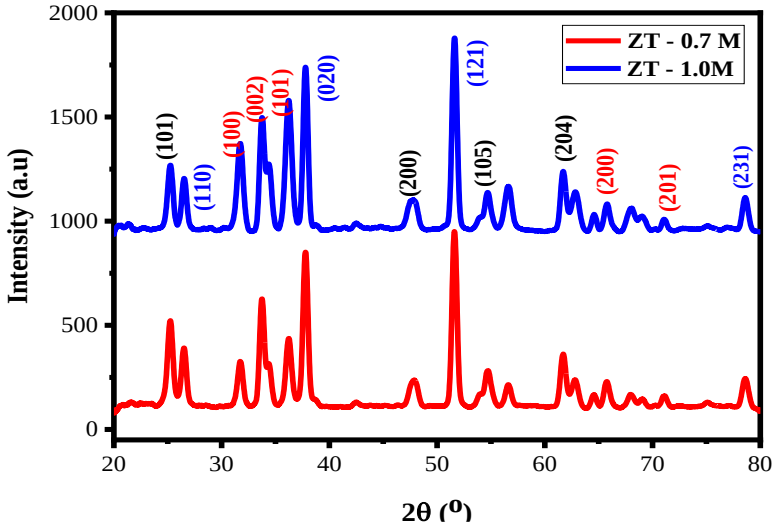

Figure 11. XRD patterns of ZnO NRs/TiO_2 composite grown from seed layer of 0.7M and 1.0M

EDX Spectroscopy

Energy Dispersive X-ray (EDX) spectra of the samples and the respective weight percentages of major and minor elements existing in the samples were also presented in Figure 12. The observed peaks confirm the presence of all expected elements, but a small amount of carbon may also arise due to the organic compound in the solution. The results support that the synthesized material is in good stoichiometry and it's in agreement with the chemical composition of the respective compound.

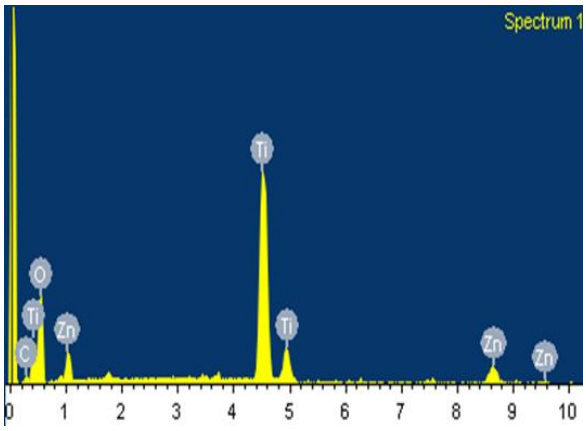

Element	Weight%	Atomic%
C K	1.95	4.19
O K	40.79	65.85
Ti K	50.88	27.44
Zn L	6.38	2.52
Totals	100.00	

Figure 12. EDX of ZnO NRs – TiO_2 composite grown from seed layer of 1.0M

AFM analysis

Atomic force microscopy (AFM) is an important means to determine the information on the material surface. Here we use AFM to analyze the changes on the surface of the samples after irradiation. Figure 13 is the image of the samples at the same initial condition formed at different solution concentrations of the seed layer. The roughness values obtained from the AFM analysis of the two photoanode samples were presented in Table 1. The thin films' surface roughness is in the nanometer range and rises with crystallite size. Therefore, the surface of ZT – 1.0 can be expected to have higher efficiency due to higher roughness for its potential to better adsorption and absorption of dye.

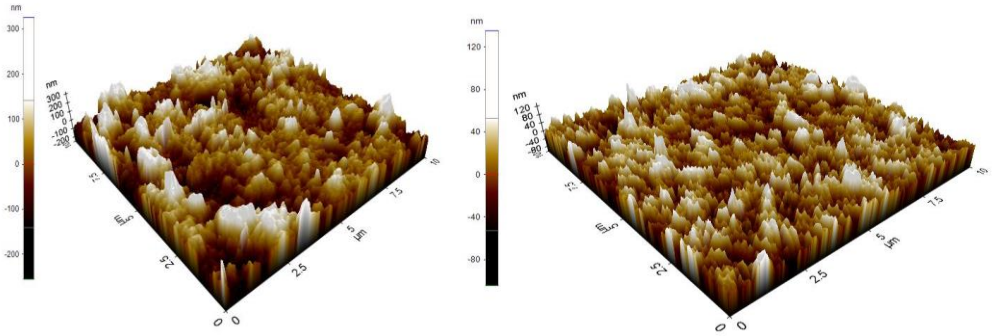

Figure 13. AFM for ZnO NRs/TiO_2 composite grown from seed layer of (a) 0.7M (b) 1.0M

Table 1. Roughness information of ZnO NRs/TiO2 composite grown from seed layer of (a) 0.7M (b) 1.0M

ZnO Conc. (M)	RMS roughness R_q (nm)	Roughness average R_a (nm)
0.7	11.667	9.579
1.0	16.429	12.886

Optical analysis

Optical characterization of nanocomposite thin films gives more information about absorbance, transmittance, optical band gap, band structure, etc. It was known that the increased light absorption permitted either the creation of electron-hole pairs or atomic vibration or plasmonic effects. If the former behavior occurs, the photo-induced current will certainly increase (Nagendra et al., 2017). Figure 14 is the absorption spectra of ZnO nanorods/TiO_2. As can be seen, the sample consisting of ZnO nanorods/TiO_2 absorption is more in the UV spectrum. This means that the electron is excited from the valance to the conduction band if a photon of energy given to the electron is equal to or higher than the optical band gap energy (Khan, 2017). Therefore it can be a promising candidate for utilization in solar cells. Zarghami et al., (2016) reported that a sample with a higher absorption edge would absorb more spectrum than one with less.

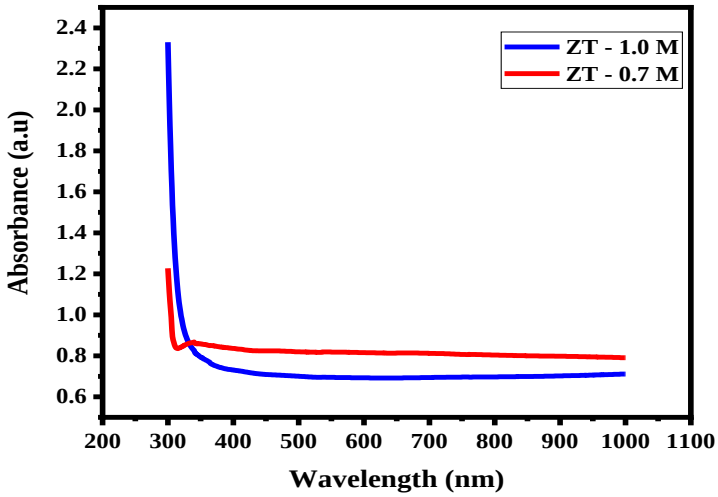

Figure 14. UV-Vis absorption spectra of ZnO NRs/TiO_2 composite grown from seed layer of 0.7M and 1.0M

The relation between transmittance spectra and wavelength is clearly shown in Figure 15; the transmittance value grows quickly within the domain (300-400nm), and then the values move constantly. The high transmittance is in a visible wavelength region, and a sharp absorption edge is observed in the film. It is clear that a lower transmittance is observed for these samples. The transmittance value of ZT – 0.7M are slightly lower than those for ZT – 1.0M, which may be due to the greater reflection or scattering effect in sample and worse crystallinity (Nykyruy et al., 2019).

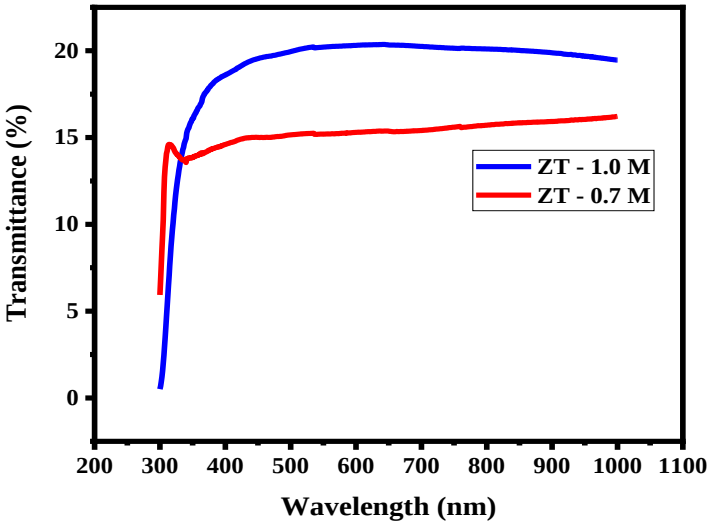

Figure 15. Plot of transmittance versus wavelength for ZnO NRs/TiO2 composite grown from seed layer of 0.7M and 1.0M

The changes produced in the band gap of ZT samples as a function of molarities are given in Figure 16. The corresponding band gaps of the nanostructures were calculated from the UV-Vis absorbance spectra using the Tauc equation (Singh et al., 2020).

$$(\alpha hv) = A\left(hv - E_g\right)^n \quad (13)$$

Where υ is the angular frequency (Hz), A is constant, Eg is the optical band gap (eV), and n is constant.

The intercept on the $hv - axis$ of the Tauc plot $(\alpha hv)^n$ Versus hv gives the band gap energy of the samples. It was seen that the estimated optical band gap of ZT-1.0M is 3.84 eV; this is smaller than the band gap of ZT- 0.7M of value 3.924 eV; this means that the later sample exhibits significantly higher energy of electron transition than ZT – 1.0M. However, the two sample values are greater than the theoretical band gap of ZnO and TiO_2. The variation in band gap may be due interaction between TiO_2 and ZnO forming an impurity band, which shifts the Fermi level; this offer to band-gap lessening (Singh et al., 2017). As a result, the optical absorption edge's shift into the visible range enables ZnO/TiO_2 nanocomposites photoactivity under visible light irradiation (Savari et al., 2021).

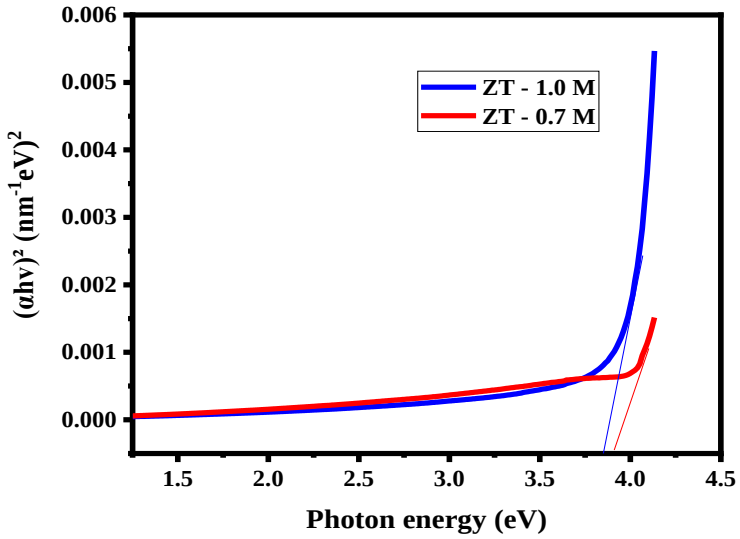

Figure 16. The plot of versus photon energy for ZnO NRs/TiO_2 composite grown from seed layer of 0.7M and 1.0M

Performance of the DSSC

Figure 17. Present the photocurrent density voltage curve for the samples with working electrodes with ZnO NRs/TiO2 composite grown from different seed layers. It was remarked in Table 2 that the efficiency of cell developed with photoanode of ZT – 0.7 M is 0.6469 %, and ZT – 1.0 M is 0.7645 %. Clearly, ZT – 1.0 M photoanode gives better efficiency. The enhanced efficiency has been attributed due to high photocurrents and faster electron transportation in ZT – 1.0M sample. It was clarified in many literature that electrodes with morphology inform of

nanorods have chances to improve the performance of dye synthesis solar cells, as it could provide a smooth path, fast photoelectrons ferry and reduced electrons holes recombination (Selvapriya et al., 2019), (Manthina et al., 2012). Also, a porous structure offers higher dye absorption (Li et al., 2015) because it may act as an electron pathway that results in longer charge migration routes (Ramli, 2017). The lower performance of DSSC is due to the occurrence of dark current. This is a phenomenon in which electrons generated from dye into electrolyte recombined with holes. Therefore present configuration is a significant step for producing cells with high performance.

Table 2. Dependence of DSSC efficiency with different precursor concentrations of seed layer

Device	I_{max} (mA)	V_{max} (mV)	J_{sc} (mA)	V_{oc} (mV)	FF%	η (%)
ZT-0.7M	0.00051644	0.31315000	2.95139300	0.44186812	49.60	0.6469
ZT-1.0M	0.00076648	0.24936023	4.38656200	0.42179566	41.32	0.7645

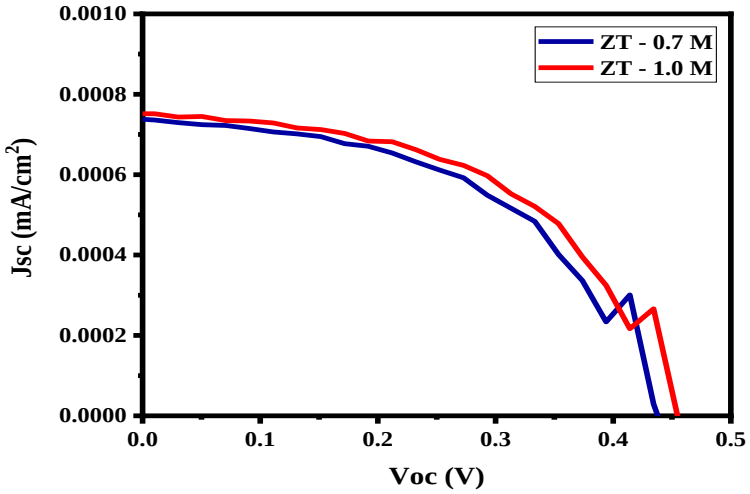

Figure 17. J-V curve for ZnO NRs/TiO_2 based DSSC grown from seed layer of 0.7M and 1.0M

CONCLUSION

The present study presents an experimental approach on several key themes that aim to optimize photoanode for dye synthesis solar cells. Firstly, we illustrate the spraying of TiO2 on aligned ZnO nanorods grown from ZnO layer. The layer of ZnO nanoparticles and nanorods were developed using spin coating and hydrothermal methods, respectively. Field emission scanning electron microscopy studies yields different morphologies. From the pictures, merely, the optimum deposition parameters of the seed layer of molarity 1.0M that yield ZnO nanorods of high uniformity and dense collections were achieved by dissolving 2.195g of Zinc acetate dihydrate $(Zn(CH_3COO)_2.(H_2O)_2$, and 1.0519g of diethanolamine $HN(CH_2CH_2OH)$ in 10 ml ethanol. The cross-sectional image confirmed that ZnO was grown vertically on substrates. The EDX spectrum reveals that the combined film comprises Zn, O, Ti and a small quantity of C. All the AFM images

of synthesized ZnO NRs/TiO_2 show a columnar shape with a well-defined rough surface. The XRD pattern revealed that the films contain ZnO nanorod and exhibit a wurtzite structure with a preferred (002) plane; in addition, TiO2 was also noticed with the strongest peak in the (101) plane.

We observed a quantified band gap of ZT - 1.0 M and ZT - 0.7 M from the optical properties measurement result as 3.84 eV and 3.92 eV, respectively. The differences may be attributed to changes in crystalline size. In the investigation of optical properties, high transmittance in the visible region was witnessed and was found to be higher with the increase of molarity concentration. In comparison, the absorbance spectra are high in the UV region. The results indicated that the fabricated photoanode with code ZT – 1.0 M had enhanced structural, optical and electrical properties and are a good promise for enhancing the efficiency of DSSC applications. The reason may be due to the advantage it took from the characteristics of both structures (ZnO and TiO_2), the high surface area of the nanoparticles and the high electron transport characteristics of the 1-D structures. Therefore, work demonstrated that ZT composite electrodes foresee the number of progresses for rapid charge transfer and larger specific surface area recombination control for good cell performance. Although the work is a better way of producing efficiency, the result is still low. Serious optimization of photoanode is required to enhance the DSSC's efficiency.

REFERENCES

Adams, S., & Nsiah, C. (2019). Reducing carbon dioxide emissions; Does renewable energy matter? *Science of the Total Environment*, *693*, 133288. https://doi.org/10.1016/j.scitotenv.2019.07.094

Akinoglu, B. G., Tuncel, B., & Badescu, V. (2021). Beyond 3rd generation solar cells and the full spectrum project. Recent advances and new emerging solar cells. *Sustainable Energy Technologies and Assessments*, *46*(3), 101287. https://doi.org/10.1016/j.seta.2021.101287

Ali, S. M., Farooq, W. A., Baig, M. R., Shar, M. A., Atif, M., Alghamdi, S. S., AlGarawi, M. S., Naeem-Ur-Rehman, & Aziz, M. H. (2015). Structural and optical properties of pure and Ag doped ZnO thin films obtained by sol gel spin coating technique. *Materials Science- Poland*, *33*(3), 601–605. https://doi.org/10.1515/msp-2015-0091

Al-Kahlout, A. (2015). Thermal treatment optimization of ZnO nanoparticles-photoelectrodes for high photovoltaic performance of dye-sensitized solar cells. *Journal of the Association of Arab Universities for Basic and Applied Sciences*, *17*, 66–72. https://doi.org/10.1016/j.jaubas.2014.02.004

Bakr, N. A., Khalaf Ali, A., Ali, A. K., Jassim, S. M., & Hasoon, K. I. (2017). Effect of N719 Dye Concentration on the Conversion Efficiency of Dye Sensitized Solar Cells ZANCO Journal of Pure and Applied. *ZANCO Journal of Pure and Applied*, *29*(2), 274–280. https://www.researchgate.net/publication/322887459

Boro, B., Gogoi, B., Rajbongshi, B. M., & Ramchiary, A. (2018). Nanostructured TiO2/ZnO nanocomposite for dye-sensitized solar cells application: A review. *Renewable and Sustainable Energy Reviews*, *81*(1), 2264–2270. https://doi.org/10.1016/j.rser.2017.06.035

Chou, J. C., Ko, C. C., Kuo, P. Y., Lai, C. H., Nien, Y. H., & Chang, J. X. (2019). Fabrication of Dye-Sensitized Solar Cells Using Zinc Oxide Nanorod-Modified Titanium Dioxide Photoanode. *IEEE Transactions on Nanotechnology*, *18*, 553–561. https://doi.org/10.1109/TNANO.2019.2915367

Dodoo-Arhin, D., Buabeng, F. P., Mwabora, J. M., Amaniampong, P. N., Agbe, H., Nyankson, E., Obada, D. O., & Asiedu, N. Y. (2018). The effect of titanium dioxide synthesis technique and its photocatalytic degradation of organic dye pollutants. *Heliyon*, *4*(7), e00681. https://doi.org/10.1016/j.heliyon.2018.e00681

Edalati, K., Shakiba, A., Vahdati-Khaki, J., & Zebarjad, S. M. (2016). Low-temperature hydrothermal synthesis of ZnO nanorods: Effects of zinc salt concentration, various solvents and alkaline mineralizers. *Materials Research Bulletin*, *74*, 374–379. https://doi.org/10.1016/j.materresbull.2015.11.001

Ejovwokoghene, J., Iyuke, S. E., Daramola, M., & Oyetunde, O. A. (2020). Synthesis of improved dye-sensitized solar cell for renewable energy power generation. *Solar Energy*, *206*, 918–934. https://doi.org/10.1016/j.solener.2020.05.002

Hezam, M., Algarni, A., Ghaithan, H., Alzahrani, H., & Alshehri, A. (2021). *Hydrothermal growth optimization of vertically aligned ZnO nanowire arrays and their dye- sensitized solar cell performance under air / oxygen environments Hydrothermal growth optimization of vertically aligned ZnO nanowire arrays and their dye-sensitized*. *8*, 105501.

Humayun, M., Raziq, F., Khan, A., & Luo, W. (2018). Modification strategies of TiO2 for potential applications in photocatalysis: A critical review. *Green Chemistry Letters and Reviews*, *11*(2), 86–102. https://doi.org/10.1080/17518253.2018.1440324

Inamdar, S. I., Ganbavle, V. V., & Rajpure, K. Y. (2014). ZnO based visible-blind UV photodetector by spray pyrolysis. *Superlattices and Microstructures*, *76*, 253–263. https://doi.org/10.1016/j.spmi.2014.09.041

Iqbal, M. Z., Ali, S. R., & Khan, S. (2019). Progress in dye sensitized solar cell by incorporating natural photosensitizers. *Solar Energy*, *181*(2), 490–509. https://doi.org/10.1016/j.solener.2019.02.023

John K, A., Naduvath, J., Mallick, S., Pledger, J. W., Remillard, S. K., DeYoung, P. A., Thankamoniamma, M., Shripathi, T., & Philip, R. R. (2016). Electrochemical Synthesis of Novel Zn-Doped TiO2 Nanotube/ZnO Nanoflake Heterostructure with Enhanced DSSC Efficiency. *Nano-Micro Letters*, *8*(4), 381–387. https://doi.org/10.1007/s40820-016-0099-z

Khalid Hossain, M., Pervez, M. F., Mia, M. N. H., Tayyaba, S., Jalal Uddin, M., Ahamed, R., Khan, R. A., Hoq, M., Khan, M. A., & Ahmed, F. (2017). Annealing temperature effect on structural, morphological and optical parameters of mesoporous TiO2 film photoanode for dye-sensitized solar cell application. *Materials Science- Poland*, *35*(4), 868–877. https://doi.org/10.1515/msp-2017-0082

Li, F., Jiao, Y., Xie, S., & Li, J. (2015). Sponge-like porous TiO2/ZnO nanodonuts for high efficiency dye-sensitized solar cells. *Journal of Power Sources*, *280*, 373–378. https://doi.org/10.1016/j.jpowsour.2015.01.118

Maçaira, J., Andrade, L., & Mendes, A. (2013). Review on nanostructured photoelectrodes for next generation dye-sensitized solar cells. *Renewable and Sustainable Energy Reviews*, *27*, 334–349. https://doi.org/10.1016/j.rser.2013.07.011

Manthina, V., Correa Baena, J. P., Liu, G., & Agrios, A. G. (2012). ZnO-TiO2 nanocomposite films for high light harvesting efficiency and fast electron transport in dye-sensitized solar cells. *Journal of Physical Chemistry C*, *116*(45), 23864–23870. https://doi.org/10.1021/jp304622d

Mehmood, U., Al-Ahmed, A., Al-Sulaiman, F. A., Malik, M. I., Shehzad, F., & Khan, A. U. H. (2017). Effect of temperature on the photovoltaic performance and stability of solid-state

dye-sensitized solar cells: A review. *Renewable and Sustainable Energy Reviews*, *79*(April), 946–959. https://doi.org/10.1016/j.rser.2017.05.114

Mousa, H. M., Alenezi, J. F., Mohamed, I. M. A., Yasin, A. S., Hashem, A. F. M., & Abdal-hay, A. (2021). Synthesis of TiO2@ZnO heterojunction for dye photodegradation and wastewater treatment. *Journal of Alloys and Compounds*, *886*, 161169. https://doi.org/10.1016/j.jallcom.2021.161169

Mustafa, M. K., Iqbal, Y., Majeed, U., & Sahdan, M. Z. (2017). Effect of P recursor' s Concentration on Structure and Morphology of ZnO Nanorods Synthesized Through Hydrothermal Method on Gold Surface. *AIP Conference Proceedings*, *030120*. https://doi.org/10.1063/1.4968373

Nagendra Vara Prasad M, M. R. Y. and J. K. R. (2017). Effect of Deposition Temperature on the Physical Properties of Ag-Cu2O Thin Films by D C Magnetron Sputtering. *Int. Journal of Engineering Research and Application*, *7*(10), 11–14. https://doi.org/10.1016/j.spmi.2017.02.003

Nykyruy, L. I., Yavorskyi, R. S., Zapukhlyak, Z. R., Wisz, G., & Potera, P. (2019). Evaluation of CdS/CdTe thin film solar cells: SCAPS thickness simulation and analysis of optical properties. *Optical Materials*, *92*(3), 319–329. https://doi.org/10.1016/j.optmat.2019.04.029

Ossai, A. N., Alabi, A. B., Ezike, S. C., & Aina, A. O. (2020). Zinc oxide-based dye-sensitized solar cells using natural and synthetic sensitizers. *Current Research in Green and Sustainable Chemistry*, *3*(12), 100043. https://doi.org/10.1016/j.crgsc.2020.100043

Padmini, M., Balaganapathi, T., & Thilakan, P. (2021). Mesoporous rutile TiO2: Synthesis, characterization and photocatalytic performance studies. *Materials Research Bulletin*, *144*(July), 111480. https://doi.org/10.1016/j.materresbull.2021.111480

Parisi, A., Pernice, R., Andò, A., Cino, A. C., Franzitta, V., & Busacca, A. C. (2017). Electro-optical characterization of ruthenium-based dye sensitized solar cells: A study of light soaking, ageing and temperature effects. *Optik*, *135*, 227–237. https://doi.org/10.1016/j.ijleo.2017.01.100

Rahman, F. A., Aziz, M. M. A., Saidur, R., Bakar, W. A. W. A., Hainin, M. R., Putrajaya, R., & Hassan, N. A. (2017). Pollution to solution: Capture and sequestration of carbon dioxide (CO2) and its utilization as a renewable energy source for a sustainable future. *Renewable and Sustainable Energy Reviews*, *71*(January), 112–126. https://doi.org/10.1016/j.rser.2017.01.011

Rajan, A. K., & Cindrella, L. (2019). Ameliorating the photovoltaic conversion efficiency of ZnO nanorod based dye-sensitized solar cells by strontium doping. *Superlattices and Microstructures*, *128*, 14–22. https://doi.org/10.1016/j.spmi.2019.01.005

Resmini, A., Tredici, I. G., Cantalini, C., Giancaterini, L., De Angelis, F., Rondanina, E., Patrini, M., Bajoni, D., & Anselmi-Tamburini, U. (2015). A simple all-solution approach to the synthesis of large ZnO nanorod networks. *Journal of Materials Chemistry A*, *3*(8), 4568–4577. https://doi.org/10.1039/c4ta05207b

Rui, Y., Xiong, H., Su, B., Wang, H., Zhang, Q., Xu, J., & Müller-buschbaum, P. (2017). Electrochimica Acta Liquid-liquid interface assisted synthesis of SnO 2 nanorods with tunable length for enhanced performance in dye-sensitized solar cells. *Electrochimica Acta*, *227*, 49–60. https://doi.org/10.1016/j.electacta.2017.01.004

Savari, R., Rouhi, J., Fakhar, O., Kakooei, S., Pourzadeh, D., Jahanbakhsh, O., & Shojaei, S. (2021). Development of photo-anodes based on strontium doped zinc oxide-reduced graphene oxide nanocomposites for improving performance of dye-sensitized solar cells.

Ceramics International, *47*(22), 31927–31939. https://doi.org/10.1016/j.ceramint.2021.08.079

Selvapriya, R., Mayandi, J., Ragavendran, V., Sasirekha, V., Vinodhini, J., & Pearce, J. M. (2019). Dual morphology titanium dioxide for dye sensitized solar cells. *Ceramics International*, *45*(6), 7268–7277. https://doi.org/10.1016/j.ceramint.2019.01.008

Sharma, S., Bulkesh Siwach, Ghoshal, S. K., & Mohan, D. (2017). Dye sensitized solar cells: From genesis to recent drifts. *Renewable and Sustainable Energy Reviews*, *70*(July 2015), 529–537. https://doi.org/10.1016/j.rser.2016.11.136

Singh, A., Mohan, D., Ahlawat, D. S., & Richa. (2017). Performances of spin coated silver doped ZnO photoanode based dye sensitized solar cell. *Processing and Application of Ceramics*, *11*(3), 213–219. https://doi.org/10.2298/PAC1703213S

Singh, S. K., Dutta, D., Das, S., Dhar, A., & Paul, M. C. (2020). Synthetic and structural investigation of ZnO nanorods, hydrothermally grown over Au coated optical fiber for evanescent field-based detection of aqueous ammonia. *Materials Science in Semiconductor Processing*, *107*(6), 104819. https://doi.org/10.1016/j.mssp.2019.104819

Song, H., Ho Jeong, H., Hoon Song, J., Woo Shin, S., Chun, J., Ju Park, S., Sun Won, Y., & Young Jung, G. (2014). Fabrication of glass-free photoelectrodes for dye-sensitized solar cells (DSSCs) by transfer method using ZnO nanorods sacrificial layer. *Materials Letters*, *132*, 27–30. https://doi.org/10.1016/j.matlet.2014.06.032

Sugathan, V., John, E., & Sudhakar, K. (2015). Recent improvements in dye sensitized solar cells: A review. *Renewable and Sustainable Energy Reviews*, *52*, 54–64. https://doi.org/10.1016/j.rser.2015.07.076

Tan, H. J., Zainal, Z., Talib, Z. A., Lim, H. N., Shafie, S., Tan, S. T., Tan, K. B., & Bahrudin, N. N. (2021). Synthesis of high quality hydrothermally grown ZnO nanorods for photoelectrochemical cell electrode. *Ceramics International*, *47*(10), 14194–14207. https://doi.org/10.1016/j.ceramint.2021.02.005

Tiwari, A., Shukla, A., Tiwari, D., Choi, S. S., Shin, H. G., & Lee, S. M. (2019). Titanium dioxide nanomaterials and its derivatives in the remediation of water: Past, present and future. *Applied Chemistry for Engineering*, *30*(3), 261–279. https://doi.org/10.14478/ace.2019.1035

Tyagi, J., Gupta, H., & Purohit, L. P. (2021). Mesoporous ZnO/TiO2 photoanodes for quantum dot sensitized solar cell. *Optical Materials*, *115*(March), 111014. https://doi.org/10.1016/j.optmat.2021.111014

Yan, X., & Chen, X. (2012). Titanium Dioxide Nanomaterials. In *Materials Research Society Symposium Proceedings* (Vol. 1352, Issue June 2015). https://doi.org/10.1002/9781119951438.eibc2335

Zainal, S. M., Zamzuri, M., Hasnulhadi, M., Nazree, M., Fariza, M., & Izaki, M. (2018). Characterization of single layer ZnO thin films prepared by sol-gel spin coating technique at different concentration. *Indian Journal of Public Health Research and Development*, *9*(12), 2620–2625. https://doi.org/10.5958/0976-5506.2018.02110.1

Zarghami, Z., Ramezani, M., & Motevalli, K. (2016). Zno Nanorods/Nanoparticles: Novel Hydrothermal Synthesis, Characterization and Formation Mechanism for Increasing the Efficiency of Dye-Sensitized Solar Cells. *Journal of Cluster Science*, *27*(4), 1451–1462. https://doi.org/10.1007/s10876-016-1011-1